^{11}B NMR studies of the electronic and magnetic properties of $LuRh_4B_4$ and $GdRh_4B_4$

D. C. Johnston and B. G. Silbernagel
Exxon Research-Engineering Co., P.O. Box 45, Linden, New Jersey 07036
(Received 5 November 1979)

The ^{11}B NMR of two members of the (rare earth) Rh_4B_4 series of ternary metals has been examined using wide-line techniques on powdered samples at frequencies from 6–27 MHz and temperatures of 90–300 K. In $LuRh_4B_4$, satellite pairs ($\pm\frac{3}{2} \leftrightarrow \pm\frac{1}{2}$ transitions) flank a narrow central resonance ($\pm\frac{1}{2} \leftrightarrow \mp\frac{1}{2}$ transitions). From these quadrupolar satellites, we find $e^2qQ/h = 523$ kHz and $\eta = 0.37$. The central transition has isotropic, $K_{iso} = +0.013\%$, and anisotropic, $K_{anis} = -0.124\%$, components to the Knight shift; the magnitude of K_{iso} as well as the residual linewidth are in agreement with our calculated values. The magnitude of K_{anis} is much larger than previously observed for ^{11}B. The spectra are independent of temperature in the range 90–300 K, in contrast to the reported strong temperature dependence of the static susceptibility for this material. Magnetic interactions broaden the ^{11}B NMR for $GdRh_4B_4$. Paramagnetic shifts for the central component of $K_{iso} = -0.263\%$ and $K_{anis} = -0.56\%$ are seen; the calculated interactions between the ^{11}B nuclei and the Gd^{3+} magnetic moments are sufficient to account for both K_{iso} and K_{anis}. From the observed satellite structure, we estimate $e^2qQ/h = 345$ kHz, indicating that the electrostatic environment at the B sites is similar to that in $LuRh_4B_4$.

I. INTRODUCTION

The ternary rare-earth (R) classes of compounds $RMo_6(S,Se)_8$ (Refs. 1 and 2) and RRh_4B_4 (Refs. 3 and 4) have recently afforded the opportunity to explore the interaction between superconductivity and long-range magnetic ordering.[5–12] Investigations of the rhombohedral compounds $RMo_6(S,Se)_8$ have shown that long-range *antiferromagnetic* ordering of the R ions occurs in several members at temperatures T_m below the superconducting transition temperatures T_s, and that the two cooperative phenomena *coexist* below T_m.[5–8] In contrast, $HoMo_6S_8$ and $ErRh_4B_4$ exhibit long-range *ferromagnetic* order at $T_m < T_s$, and in each case the superconductivity is *quenched* below T_m.[9–12] This interplay between superconductivity and long-range magnetic ordering, which at this writing has been observed only in ternary systems, continues to be of both experimental and theoretical interest. In the present paper, we report NMR studies of ^{11}B in $LuRh_4B_4$ and $GdRh_4B_4$ which were carried out to clarify the microscopic magnetic and electrostatic properties of the RRh_4B_4 class of materials in the vicinity of the boron atoms.[13] An additional motivation was to see if the microscopic properties showed distinct deviations from past observations on binary systems containing boron in an attempt to assess why only ternary systems have thus far exhibited the coupled superconducting-magnetic phenomena described above. Nonmagnetic $LuRh_4B_4$ was chosen for examination since the Lu-Rh-B phase diagram in the vicinity of the composition $LuRh_4B_4$ has been the subject of detailed study,[14] the heat capacity and magnetic susceptibility have been measured,[15] and band-structure calculations have been carried out for this material.[16–18] $GdRh_4B_4$ was chosen as the complementary magnetic member of the series because of the particularly simple S-state form of the Gd magnetic moment.

II. EXPERIMENTAL DETAILS

The samples were synthesized by arc melting the high-purity elements in a zirconium-gettered argon atmosphere, followed by annealing in sealed Ta tubes under Ar at 1150 °C for 6 days and 800 °C for 26 h for $LuRh_4B_4$, and at 1200 °C for 6 days and 800 °C for 21 days for $GdRh_4B_4$. The inductively measured T_s of the $LuRh_4B_4$ sample was 11.28 K with a transition width of 0.03 K. The 6–7-g annealed ingots were ground and passed through a 200-mesh sieve. X-ray examination showed $\lesssim 5\%$ impurity phases in each sample. NMR observations were made with a Varian WL-112 NMR spectrometer operating at frequencies of 6–25 MHz and temperatures of 90–300 K. A Me_2CO solution of $Bu_3NH^+BF_4^-$ was used as the reference in the Knight-shift measurements.

III. RESULTS

For both materials, the ^{11}B NMR spectrum consists of a relatively narrow central component from the ($\pm\frac{1}{2} \leftrightarrow \mp\frac{1}{2}$) transitions flanked by satellites from the ($\pm\frac{3}{2} \leftrightarrow \pm\frac{1}{2}$) transitions. The central component of

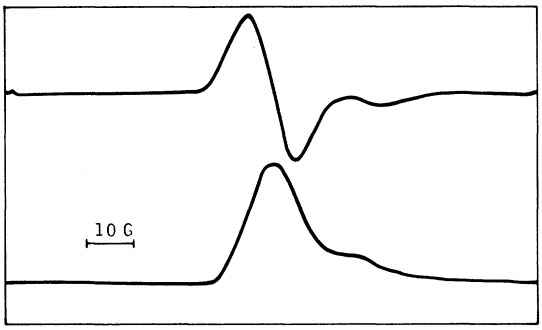

FIG. 1. A 100-G NMR scan of the absorbtion and its derivative for the $(\pm\frac{1}{2} \leftrightarrow \mp\frac{1}{2})$ transition in $LuRh_4B_4$. The asymmetry of the line indicates an anisotropic Knight shift.

the $LuRh_4B_4$ absorption spectrum and its derivative observed at a resonance frequency of 23 MHz (corresponding to an applied field of 16.8 kG) are shown in Fig. 1. The line is anisotropic, the anisotropy being proportional to the applied magnetic field strength. At low fields, a field-independent residual splitting between the maxima of the derivative curve of 6.2 G is observed. Applying a conventional form for anisotropic Knight shifts

$$\Delta H/H = K_{iso} + K_{anis}(3\cos^2\Theta - 1)/2 \ , \qquad (1)$$

to the present NMR powder spectrum, we find $K_{iso} = +0.013 \pm 0.003\%$ and $K_{anis} = -0.124 \pm 0.003\%$. No change in these shift values with temperature was observed between 300 and 90 K.

A broader magnetic field scan (Fig. 2) shows the satellite structure from the $(\pm\frac{3}{2} \leftrightarrow \pm\frac{1}{2})$ transitions. In this 1-kG scan, the derivative of the absorption is shown at two levels of gain. Two maxima and a zero crossing are seen on either side of the central component; the splitting between these features is independent of applied magnetic field strength, indicating that they are the first-order quadrupole satellites of these transitions. The maxima in the derivative curve correspond to shoulders in the powder absorption spectrum of the sample, while the zero crossing corresponds to a maximum in the absorption. The existence of two shoulders is an indication that the electric field gradient has significant nonaxial character. A conventional analysis of the spectrum yields a quadrupolar coupling constant (e^2qQ/h) of 523 ± 30 kHz and an electric-field-gradient anisotropy term (η) of 0.37 ± 0.03.

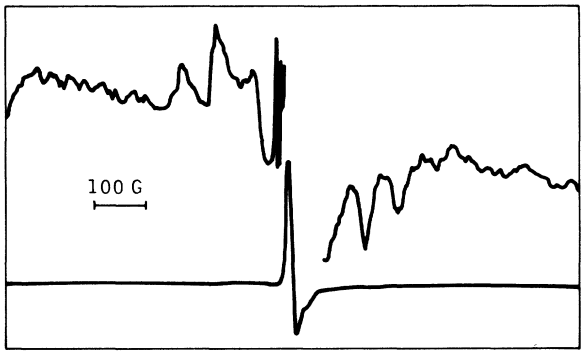

FIG. 2. A 1-kG NMR scan of the derivative of the absorption curve in $LuRh_4B_4$. Two levels of gain are shown to portray the central component (as in Fig. 1) and the satellites associated with $(\pm\frac{3}{2} \leftrightarrow \pm\frac{1}{2})$ transitions.

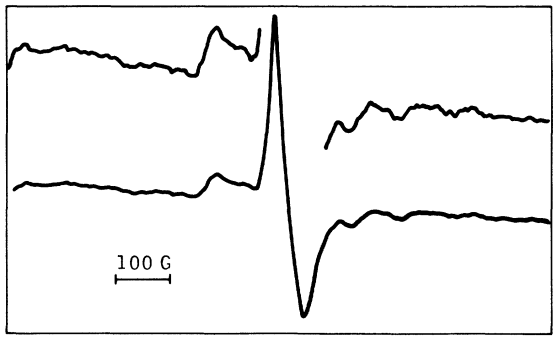

FIG. 3. A 1-kG NMR scan of the absorption derivative for $GdRh_4B_4$ reveals considerably less articulation of the satellite features and significant shifting of their positions—the result of magnetic effects.

The corresponding spectrum for $GdRh_4B_4$ shows somewhat less articulation, most likely a result of considerably broader ^{11}B NMR lines. A spectrum acquired at a relatively low frequency, 12 MHz (applied field 8.8 kG) is shown in Fig. 3. The satellite peaks observed in this case are not symmetrically disposed about the central transition, the result of combined quadrupolar and magnetic effects. The satellites are even more strongly smeared at high fields. The quadrupolar coupling constant can be estimated from the

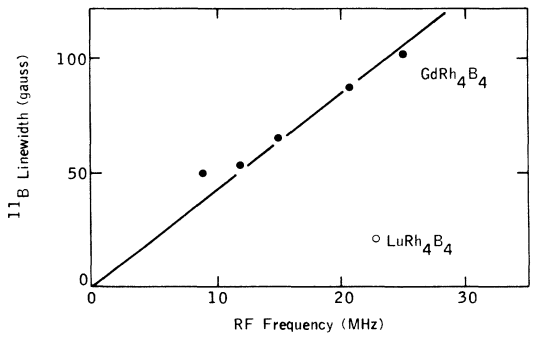

FIG. 4. The linewidth of the central component in the NMR spectrum of $GdRh_4B_4$ varies linearly at high fields. Magnetic interactions make it significantly broader than in $LuRh_4B_4$.

TABLE I. ^{11}B NMR properties of $LuRh_4B_4$ and $GdRh_4B_4$. Errors for the last digits of each quantity are in parentheses.

	K_{iso} (%)	K_{anis} (%)	e^2qQ/h (kHz)	η	ΔH residual (G)
$LuRh_4B_4$	+0.013(3)	−0.124(3)	523(30)	0.37(3)	6.2
$GdRh_4B_4$	−0.263(25)	−0.56(5)	(345)[a]	...	50

[a]Estimated.

position of the more remote satellites to be $e^2qQ/h \sim 350$ kHz, comparable to but apparently somewhat smaller than that encountered in $LuRh_4B_4$. Comparison of Figs. 2 and 3 indicates that the central component of the resonance line is much greater in $GdRh_4B_4$. As for $LuRh_4B_4$, the linewidth at high fields increases linearly with applied magnetic field, as shown in Fig. 4, where the width is plotted as a function of frequency from 9–25 MHz (6.6–18.3 kG). The linewidth is very large at the highest fields, greater than 100 G, and has a low-field residual value of ~50 G, nearly an order of magnitude larger than in the $LuRh_4B_4$ case. Shift analysis for $GdRh_4B_4$ yields $K_{iso} = -0.26 \pm 0.025\%$ and $K_{anis} = -0.56 \pm 0.045\%$. These experimental results are summarized in Table I.

IV. ANALYSIS AND DISCUSSION

The qualitative features of our results will first be discussed in the context of previous ^{11}B NMR studies and the known properties of the RRh_4B_4 materials, followed by a more detailed analysis of certain aspects of our data. In $LuRh_4B_4$, the small value of K_{iso} is quite comparable to those observed in previous studies of metallic binary and ternary systems containing boron,[19] although in the majority of other cases K_{iso} is negative rather than positive as observed here. The magnitude of e^2qQ/h, 523 kHz, lies in the intermediate range and the anisotropy factor, $\eta \simeq 0.37$, is relatively large. The most striking aspect of the anisotropic effects is the large value for K_{anis} of −0.124% which is very large by comparison with previous reports. These observations are consistent with the monoclinic-point-group symmetry reported for the boron positions in the RRh_4B_4 materials[4]: an anisotropic Knight shift usually occurs only for nuclei in sites of noncubic symmetry, and the nonzero anisotropy factor shows that the electrostatic environment has lower than axial symmetry. Since the nearest neighbor of a given boron atom is another boron atom only 1.8 Å away,[4] one source of the large anisotropy may be an indirect interaction with the adjacent boron atom mediated by the conduction electrons.

Another very important feature is the absence of observed temperature dependences to the width or position of the ^{11}B NMR line in the temperature range from 300 to 90 K. This is particularly striking in light of a variation of the reported magnetic susceptibility of $LuRh_4B_4$ (Ref. 15) over this temperature range, shown in Fig. 5, of nearly a factor of 2. The ^{11}B Knight shift is a measure of the microscopic susceptibility at the boron atom site, having the general form

$$K = \sum_i H_{hf}^i \chi_i \ , \tag{2}$$

where H_{hf}^i and χ_i are the hyperfine-field coupling constant at the boron site and the susceptibility of the ith class of electrons in the material, respectively. Certain contributions to the bulk susceptibility might well not contribute to a shift at the boron site. For example, in the metal-rich compound $V_{1+x}Se_2$, the excess vanadium atoms possess localized moments which do not cause significant Knight shifts for the other vanadium atoms.[20] However, the susceptibility variation seen in Fig. 5 is more suggestive of a band effect than of such isolated moments. Therefore, the temperature independence of these shifts indicates an extremely small hyperfine interaction between the

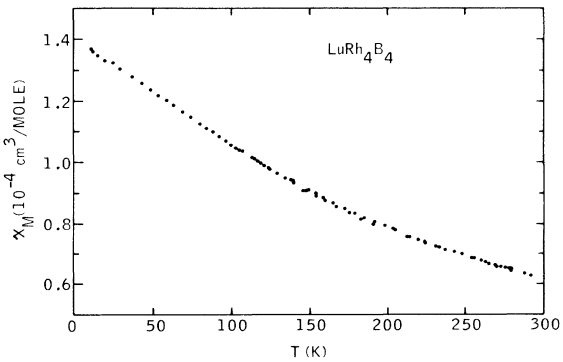

FIG. 5. The magnetic susceptibility of $LuRh_4B_4$ (from Ref. 15) has a significant temperature dependence. By contrast, almost no change is observed in the ^{11}B NMR shift or width at temperatures from 300 to 90 K, suggesting little coupling between the ^{11}B nuclei and the electrons responsible for the temperature dependence of the susceptibility.

boron nuclei and the class of conduction electrons responsible for the temperature dependence of the susceptibility.

In the case of $GdRh_4B_4$, the magnetic Gd atoms dominate the ^{11}B NMR properties. Both isotropic and anisotropic Knight shifts are large, as is the residual linewidth at low fields. Except for the presence of the anisotropy, these results are comparable to the Al NMR shifts observed in the dense rare-earth cubic-Laves-phase compounds RAl_2.[21] As in the latter cases, it appears that the Gd–Gd coupling is moderated primarily through the conduction electrons.

In the following, certain aspects of our data will be analyzed in more detail, with reference to the crystal structures of the RRh_4B_4 compounds. The RRh_4B_4 materials exhibit three polymorphic forms[4,14,22]; the preparation conditions of our samples stabilize the primitive tetragonal structure reported by Vandenberg and Matthias[4] over the other two and it is this structure with which we are concerned here. The space group is $P4_2/nmc$ (No. 137), with the atomic positions as follows (origin at $\bar{4}m2$) (Ref. 4): 2 R in 2 (b): $(0,0,\frac{1}{2})$, $(\frac{1}{2},\frac{1}{2},0)$; 8 Rh in 8 ($g$): $(0,x_{Rh},z_{Rh})$, etc., with $x_{Rh}=0.248$ and $z_{Rh}=0.137$; 8 B in 8 (g): $(0,x_B,z_B)$, etc., with $x_B=0.325$ and $z_B=0.847$. The lattice parameters are $a_0=5.294$ Å and $c_0=7.359$ Å for $LuRh_4B_4$ and $a_0=5.309$ Å and $c_0=7.417$ Å for $GdRh_4B_4$.[4]

A. Residual linewidths

We begin our analysis with a calculation of the residual linewidth of the central component ($\pm\frac{1}{2} \leftrightarrow \mp\frac{1}{2}$ transitions) of the resonance for $LuRh_4B_4$. The contribution due to dipolar interactions with neighboring nuclei can be estimated from a calculation of the second moment $M_2=\langle\Delta\omega^2\rangle$ for the resonance, which is the sum of the second-moment contributions from like neighbors (^{11}B) of spin $I=\frac{3}{2}$ and gyromagnetic ratio γ_B and unlike neighbors (^{10}B, ^{175}Lu, and ^{103}Rh) with spins denoted by S and gyromagnetic ratio γ_S. The respective contributions are[23]

$$M_2(^{11}\mathrm{B}-{}^{11}\mathrm{B})=\tfrac{9}{10}\tfrac{3}{5}\gamma_B^4\hbar^2 I(I+1)\sum_k r_k^{-6}\ , \quad (3)$$

$$M_2(^{11}\mathrm{B}-S)=\tfrac{4}{15}\gamma_B^2\gamma_S^2\hbar^2 S(S+1)\sum_k r_k^{-6}\ . \quad (4)$$

Examination of the values of $\gamma_B^2 I(I+1)$ and $\gamma_S^2 S(S+1)$ (given in Table II) shows that the ^{11}B-^{103}Rh dipolar coupling is negligible compared to the others. Therefore, only the latter lattice sums were determined. The lattice sums in Eqs. (3) and (4) were evaluated within a spherical volume about a given B atom; the sums were found to converge rapidly and approach their asymptotic values within a radius of $\sim 3a_0(\simeq 16$ Å) of the given ^{11}B atom. The lattice sums are given in Table II, along with the computed contributions to the second moment M_2, where the contributions of ^{11}B and ^{10}B to M_2 have been scaled according to their relative isotopic abundance (81% and 19%, respectively). Assuming a Gaussian line shape, the linewidth between the points of maximum slope is[24] $\Delta H_{msl}=2(M_2)^{1/2}/\gamma_B$. From Table II, we calculate $\Delta H_{msl}=4.4$ G, in reasonable agreement with the observed value of 6.2 G.

The residual linewidth of the central ^{11}B resonance due to dipolar interactions in $GdRh_4B_4$ can be es-

TABLE II. Contributions to the second moment M_2 of the central NMR resonance of ^{11}B in $LuRh_4B_4$ and $GdRh_4B_4$ due to dipolar interactions.

Nucleus or atom	γ ($G^{-1}\,sec^{-1}$)	S	$\gamma^2 S(S+1)$ ($G^{-2}\,sec^{-2}$)	$\sum_k \frac{a_0^6}{r_k^6}$	Contribution to M_2 (sec^{-2})
			$LuRh_4B_4$		
^{11}B	8583	$\frac{3}{2}$	2.763×10^8	721	3.25×10^8
^{10}B	2874	3	0.991×10^8	721	0.14×10^8
^{175}Lu	3966	$\frac{7}{2}$	2.477×10^8	95	0.23×10^8
^{103}Rh	842	$\frac{1}{2}$	0.005×10^8	. . .	. . .
			$GdRh_4B_4$		
^{157}Gd	1074	$\frac{3}{2}$	0.043×10^8	94	6×10^4
Gd^{3+}	1.757×10^7	$\frac{7}{2}$	4.86×10^{15}	94	4.46×10^{14}
^{155}Gd	804	$\frac{3}{2}$	0.024×10^8	94	4×10^4

timated in a similar fashion. Here, however, the dipolar interaction between the ^{11}B nuclei and the Gd^{3+} electronic magnetic moments ($g=2$, $S=\frac{7}{2}$, $\mu_{\rm eff}=7.94\ \mu_B$) must be included; the latter interaction is expected to be narrowed by virtue of the exchange interaction $\mathcal{H}=-2J\vec{S}_1\cdot\vec{S}_2$ between Gd electronic magnetic moments which causes ferromagnetic ordering at $T_m=5.6$ K.[3] In the absence of exchange narrowing, the residual linewidth can be calculated utilizing Eq. (4) and Table II, yielding $\Delta H_{msl}=4.9$ kG, much larger than the observed value. In the presence of exchange narrowing, the full width at half maximum power can be estimated from the following expression valid in the extreme narrowing limit $\omega_e^2 >> M_2$ (Refs. 25 and 26):

$$\Delta H=\tfrac{10}{3}(2)M_2/(\gamma_B\omega_e) \quad (5)$$

with

$$\omega_e^2=2z(J/\hbar)^2S(S+1)/3 \ , \quad (6)$$

where J is the exchange interaction constant between two Gd spins. This exchange constant will be estimated by utilizing the expression for the ferromagnetic ordering temperature T_m in the Weiss molecular-field approximation[27]:

$$J=3k_BT_m/[2zS(S+1)] \ , \quad (7)$$

where z is the number of Gd nearest neighbors to a given Gd atom, and k_B is Boltzmann's constant. In the RRh_4B_4 materials, the R atoms form a slightly distorted face-centered-cubic array,[4] so that $z=12$. Equation (7) then yields $J=6.1\times10^{-18}$ erg. From Eq. (6), $\omega_e=6.5\times10^{10}$ sec^{-1}. M_2 can be calculated by inserting the appropriate lattice sum given in Table II into Eq. (4); the result has been listed in Table II and is $M_2=4.46\times10^{14}$ sec^{-2}. Thus, the condition that $\omega_e^2 >> M_2$ is satisfied. The residual linewidth calculated for $GdRh_4B_4$ from Eq. (5) is therefore $\Delta H=5.3$ G. If the B-B dipolar contribution to the residual linewidth is included, we find $\Delta H=6.8$ G. This value is far too small to account for the residual linewidth of 50 G observed in this case. Therefore, the residual linewidth evidently arises primarily by indirect coupling between the ^{11}B nuclei and the Gd^{3+} spins via the conduction electrons.

B. Anisotropic resonance shifts

We have also estimated the dipolar contribution of the Gd electronic spins to the resonance shifts in $GdRh_4B_4$ at high applied fields. For $T >> T_m$, the local magnetic field at a boron site in the direction of the applied field due to the Gd dipoles at positions $\vec{r}_i$ with respect to the boron atom is

$$\vec{B}^{\rm loc}=[\tfrac{4}{3}\pi-\hat{M}(N)\hat{M}]\vec{M}+\vec{\mu}\sum_{r_i\le R_L} r_i^{-5}[3(\vec{r}_i\cdot\hat{\mu})^2-r_i^2] \ , \quad (8)$$

$$\equiv\Delta\vec{B}^{\rm loc}_{\rm shape}+\Delta\vec{B}^{\rm loc} \ . \quad (9)$$

Here, (N) is the demagnetization tensor, R_L is the radius of the Lorentz sphere, $\vec{M}$ is the macroscopic magnetization in the direction of the applied field, $\vec{\mu}$ is the thermal-averaged dipole moment of a Gd atom (in the direction of the applied field), and a carat over a vector signifies a unit vector expressed in terms of the unit vectors $\hat{x}$, $\hat{y}$, $\hat{z}$, along the crystal axes. The moment $\vec{\mu}$ is given by the Curie-Weiss law

$$\vec{\mu}=\frac{\mu_{\rm eff}^2\vec{H}}{3k_B(T-T_m)} \ . \quad (10)$$

$\Delta\vec{B}^{\rm loc}$ can be written as a solution to the matrix equation

$$\Delta\vec{B}^{\rm loc}=\vec{\mu}\hat{\mu}(A)\hat{\mu} \ , \quad (11)$$

where

$$A_{jk}=\sum_{r_i\le R_L}\frac{3r_{ij}r_{ik}-r_i^2\delta_{jk}}{r_i^5} \quad (12)$$

and r_{ij} is the component of $\vec{r}_i$ along the jth crystal axis. Since (A) is a symmetric, traceless tensor, $\Delta\vec{B}^{\rm loc}$ cannot give rise to an isotropic resonance shift, and therefore does not explain our observed large negative value for $K_{\rm iso}$ for $GdRh_4B_4$; this fact will appear explicitly below. $\Delta B^{\rm loc}$ does give rise, however, to anisotropic shifts which we now consider.

We have solved for the principal axes of $\Delta\vec{B}^{\rm loc}$ by diagonalizing the matrix (A). The sums appearing in Eq. (12) were evaluated within Lorentz spheres with radii up to and including $R_L=6a_0(31.854$ Å), the latter sum containing the dipolar contributions of 1281 Gd ions. The resultant principal-axis unit vectors $(\hat{P}_i)$ and eigenvalues of $\Delta\vec{B}^{\rm loc}$ $(\Delta B_i^{\rm loc})$ approach constant values for $R_L\gtrsim4a_0$ and are listed in Table III, where the principal-axis unit vectors are given in terms of the unit vectors $\hat{x}$, $\hat{y}$, and $\hat{z}$ of the lattice. Referring to Table III and noting that $P_{iz}/P_{iy}\simeq c_0/a_0$ and $-a_0/c_0$ for $i=2$ and 3, respectively, we see that the principal axis $\hat{P}_1$ of $\Delta B^{\rm loc}$ is in the [100] lattice direction, and $\hat{P}_2$ and $\hat{P}_3$ are close to the [021] and [02$\bar{1}$] lattice directions, respectively. As was anticipated above, the sum of the three eigenvalues $\Delta B_i^{\rm loc}$ is identically zero.

TABLE III. Principal-axis unit vectors $\hat{P}_i$ and corresponding eigenvalues $\Delta B_i^{\rm loc}$ of the Gd^{3+} dipolar field $\Delta\vec{B}^{\rm loc}$ at a boron site in $GdRh_4B_4$. The $\hat{P}_i$ are expressed in terms of the unit vectors of the lattice unit cell $\hat{x}$, $\hat{y}$, and $\hat{z}$; a_0 is the lattice parameter in the $\hat{x}$ and $\hat{y}$ directions (5.309 Å) (Ref. 4) and μ is the thermal average of the Gd^{3+} electronic moment in the direction of the applied field.

$\hat{P}_1=\hat{x}$	$\Delta B_1^{\rm loc}=(\mu/a_0^3)(6.5)$
$\hat{P}_2=0.582\hat{y}+0.813\hat{z}$	$\Delta B_2^{\rm loc}=(\mu/a_0^3)(4.6)$
$\hat{P}_3=-0.813\hat{y}+0.582\hat{z}$	$\Delta B_3^{\rm loc}=(\mu/a_0^3)(-11.1)$

The dependence of ΔB^{loc} on orientation of the external field with respect to the principal axes is given by Eq. (11)

$$\Delta B^{loc} = \Delta B_1^{loc}\alpha^2 + \Delta B_2^{loc}\beta^2 + \Delta B_3^{loc}\gamma^2 \ , \quad (13)$$

where α, β, and γ are the direction cosines of the field direction with respect to the principal axes: $\alpha = \sin\theta\cos\phi$, $\beta = \sin\theta\sin\phi$, and $\gamma = \cos\theta$. Utilizing the fact that $\sum_i \Delta B_i^{loc} \equiv 0$, we have transformed Eq. (13) into a form which can be compared with the experimental data

$$\Delta B^{loc} = \Delta B_3^{loc}(\tfrac{1}{2})(3\cos^2\theta - 1) + (\Delta B_1^{loc} - \Delta B_2^{loc})(\tfrac{1}{2}\sin^2\theta\cos 2\phi) \ . \quad (14)$$

From the results in Table III, and using Eqs. (10) and (11), Eq. (14) becomes

$$\frac{\Delta B^{loc}}{H} = \frac{\mu_{eff}^2}{3k_B(T - T_m)} \frac{1}{a_0^3} [-11.1(\tfrac{1}{2})(3\cos^2\theta - 1) + 1.9(\tfrac{1}{2}\sin^2\theta\cos 2\phi)] \ . \quad (15)$$

At $T = 296$ K and utilizing the values $T_m = 6$ K, $\mu_{eff} = 7.94\mu_B$, and $a_0 = 5.309$ Å, our result for the calculated anisotropic ^{11}B shifts in $GdRh_4B_4$ deriving from local dipolar fields of the Gd electronic moments is found from Eq. (15) to be

$$\Delta B^{loc}/H = (-0.33\%)(\tfrac{1}{2})(3\cos^2\theta - 1) + (0.057\%)(\tfrac{1}{2}\sin^2\theta\cos 2\phi) \ . \quad (16)$$

Referring to Table I, the first term of Eq. (16) is of the correct sign but about 41% smaller in magnitude than the measured value of K_{anis}.

Equation (9) for $\vec{B}^{loc}$ contains a term $\Delta\vec{B}_{shape}^{loc}$ dependent on the shape of the sample. Because M is not negligible at high fields for $GdRh_4B_4$ even at room temperature, and since our sample is composed of small nonspherical grains, this demagnetization term could also give rise to an appreciable contribution to our measured K_{anis} for this material; we therefore proceed to calculate its magnitude. ΔB_{shape}^{loc} can be written

$$\Delta\vec{B}_{shape}^{loc} = [\hat{M}(N')\hat{M}]\vec{M} \ , \quad (17)$$

where

$$N'_{ij} = \tfrac{4}{3}\pi\delta_{ij} - N_{ij} \ . \quad (18)$$

For an ellipsoid of revolution, (N') is a symmetric traceless tensor[28] which has the following diagonal elements with respect to the principal axes: $\frac{4}{3}\pi - N_\perp$, $\frac{4}{3}\pi - N_\perp$, and $\frac{4}{3}\pi - N_\parallel$. Using the line of reasoning preceding Eq. (14), we obtain from Eq. (17)

$$\Delta\vec{B}_{shape}^{loc} = (\tfrac{4}{3}\pi - N_\parallel)(\tfrac{1}{2})(3\cos^2\theta - 1)\vec{M} \ , \quad (19)$$

where θ is the angle between the principal axis of revolution and the applied field. To obtain an estimate of the maximum magnitude of ΔB_{shape}^{loc}, we assume that the sample particles are in the shape of thin discs, for which $(\frac{4}{3}\pi - N_\parallel) = \frac{1}{3}(-8\pi)$. Using Eq. (10) and the lattice constant data to determine that $M(300\text{ K}) = 4.3 \times 10^{-4}H$, Eq. (19) gives the following maximum value for K_{anis}^{shape}:

$$K_{anis}^{shape} = -0.36\% \ . \quad (20)$$

The combination of this term with the local dipolar contribution -0.33% found above is sufficient to account for the observed value of K_{anis} in Table I for $GdRh_4B_4$.

C. Isotropic resonance shifts

An estimate of K_{iso} for $LuRh_4B_4$ was made, based on the magnetic susceptibility data of Fig. 5 in conjunction with results of recent band-structure calculations.[16–18] From Eq. (2), the contribution to K_{iso} due to the s-electron contact-interaction term is

$$K_{iso} = H_{hf}^s \chi_s \ , \quad (21)$$

where χ_s is the s-electron contribution to the measured susceptibility, in units of μ_B/atom G, and H_{hf}^s is the hyperfine coupling constant in the inverse units. Both the temperature dependence and magnitude of the susceptibility, shown in Fig. 5, suggest that a major fraction of the total density of states at the Fermi level, $N(0)$, derives from d-band contributions. Indeed, the calculations of the room-temperature band structures of the RRh_4B_4 materials[16–18] confirm this, and further indicate that $N_s(0)/N(0) \simeq 0.04$. We therefore estimate $\chi_s \simeq 0.04(\chi - \chi^{core})$, where χ is the value measured at room temperature from Fig. 5, and χ^{core} is the diamagnetic core contribution. Correcting χ for the core correction of -1.0×10^{-4} cm^3/mole,[29] converting the units of χ to those appropriate to Eq. (21), and utilizing the free atom value of 1.0×10^6 atom G/μ_B for H_{hf}^s of ^{11}B,[30] we obtain from Eq. (21)

$$K_{iso} = +0.013\% \ .$$

The (fortuitously good) agreement between this rough estimate and the observed value in Table I is another indication that the boron atoms are only weakly coupled to the d electrons responsible for the temperature-dependent susceptibility.

Finally, we make an estimate of K_{iso} for $GdRh_4B_4$ by assuming that the isotropic shift arises solely via the s-electron contact interaction; the above agree-

ment between the calculated and observed values of K_{iso} for $LuRh_4B_4$ lends credence to this assumption. We further assume an (isotropic) exchange interaction between a Gd ion and the s-type conduction electrons, with a Hamiltonian given by

$$\mathcal{H} = -2J\vec{S}\cdot\vec{s} \ , \tag{22}$$

where J is the spin exchange coupling constant, $\vec{S}$ is the spin angular momentum of the Gd ion, and $\vec{s}$ is the s-type conduction-electron-spin density at the site of the Gd ion. This exchange interaction leads to spin polarization of the conduction electrons,[31] with a net induced conduction-electron magnetic moment per Gd ion given by[32,21]

$$\langle \mu_s \rangle = \frac{2JN_s(0)}{g}\mu_{Gd} \ , \tag{23}$$

where $N_s(0)$ is the s-electron density of states at the Fermi level for both spin directions, g is the Landé g factor for the Gd ion ($g=2$), and μ_{Gd} is the thermal-averaged value of the Gd ion magnetic moment in an applied magnetic field H. The equivalent magnetic susceptibility χ_s of the s-type conduction electrons corresponding to this induced magnetic moment is, using Eqs. (10) and (23),

$$\chi_s = \frac{2JN_s(0)}{9g\mu_B}\frac{\mu_{eff}^2}{3k_B(T-T_m)} \ , \tag{24}$$

where the factor $1/(9\mu_B)$ has been introduced so that the units of χ_s are (μ_B/atom G). Assuming a magnitude of 0.1 eV atom for $|J|$, which is typical of values obtained for s-electron-R ion exchange,[33] and using $N_s(0)=0.03$ states/eV atom from Ref. 16, $|\chi_s|$ at room temperature is found from Eq. (24) to be

$$|\chi_s(300\ \text{K})| = 2\times10^{-9}\ \mu_B/\text{atom G} \ . \tag{25}$$

Using as before the free atom value of 1.0×10^6 atom G/μ_B for the contact hyperfine coupling constant for ^{11}B, Eqs. (2) and (25) predict

$$|K_{iso}| = 0.2\% \ ,$$

of the right magnitude to explain the observed value of K_{iso} for $GdRh_4B_4$.

V. SUMMARY AND CONCLUSIONS

Both $LuRh_4B_4$ and $GdRh_4B_4$ have comparable electrostatic environments at the sites of the boron atoms, but the magnetic properties are significantly different. In $LuRh_4B_4$, the magnitude of K_{iso} is small and typical of metallic compounds containing boron, and is in agreement with the value we calculate from the contact interaction utilizing the known s-electron density of states at the Fermi level. The residual linewidth at low fields can be accounted for by dipolar broadening. However, K_{anis} is much greater than previously observed for ^{11}B and its origin appears to be B–B interactions mediated by the conduction electrons. The absence of any detectable temperature dependence between 90 and 300 K for K_{iso} and K_{anis} in spite of a large variation in the static susceptibility of the material over this temperature range suggests a very weak interaction of the ^{11}B nuclei with those conduction electrons (primarily the Rh d electrons) responsible for the temperature dependence of the susceptibility. This decoupling of certain conduction-electron classes from particular sets of atoms within a unit cell appears to be a characteristic which differentiates the ternary RRh_4B_4 and $RMo_6(S,Se)_8$ compounds from most other binary and ternary metals that do not exhibit the unusual superconducting and magnetic phenomena cited in the introduction. For the $GdRh_4B_4$ compound, the calculated magnetic-field-induced polarization of the conduction electrons by the Gd ions is of the right magnitude to account for the isotropic shift, and the sum of the calculated dipolar interactions and sample-shape effects can explain the observed high-field anisotropy; however, the detailed origin of the large residual linewidth at low fields remains unclear, but is probably due to an indirect B–Gd interaction moderated via the conduction electrons. The present investigation extends the foundation of experimental results on the ternary RRh_4B_4 compounds and in particular, has yielded microscopic evidence for several conduction-electron effects within the unit cell which may prove necessary to a detailed understanding of the collective transitions in these materials.

ACKNOWLEDGMENT

The authors thank Layce Gebhard for her expert technical assistance.

[1]Ø. Fischer, A. Treyvaud, R. Chevrel, and M. Sergent, Solid State Commun. 17, 721 (1975).
[2]R. N. Shelton, R. W. McCallum, and H. Adrian, Phys. Lett. A 56, 213 (1976).
[3]B. T. Matthias, E. Corenzwit, J. M. Vandenberg, and H. E. Barz, Proc. Nat. Acad. Sci. U.S.A. 74, 1334 (1977).
[4]J. M. Vandenberg and B. T. Matthias, Proc. Nat. Acad. Sci. U.S.A. 74, 1336 (1977).
[5]R. W. McCallum, D. C. Johnston, R. N. Shelton, W. A. Fertig, and M. B. Maple, Solid State Commun. 24, 501 (1977).
[6]J. W. Lynn, D. E. Moncton, G. Shirane, W. Thomlinson, J.

Eckert, and R. N. Shelton, BNL Report No. 23450, Conference No. 771127-10, 1977 (unpublished).
[7]M. Ishikawa and Ø. Fischer, Solid State Commun. 24, 747 (1977).
[8]D. E. Moncton, G. Shirane, W. Thomlinson, M. Ishikawa, and Ø. Fischer, Phys. Rev. Lett. 41, 1133, 1428 (1978).
[9]W. A. Fertig, D. C. Johnston, L. E. Delong, R. W. McCallum, M. B. Maple, and B. T. Matthias, Phys. Rev. Lett. 38, 987 (1977).
[10]D. E. Moncton, D. B. McWhan, J. Eckert, G. Shirane, and W. Thomlinson, Phys. Rev. Lett. 39, 1164 (1977).
[11]M. Ishikawa and Ø. Fischer, Solid State Commun. 23, 37 (1977).
[12]J. W. Lynn, D. E. Moncton, W. Thomlinson, G. Shirane, and R. N. Shelton, Solid State Commun. 26, 493 (1978).
[13]A brief account of this work has been given elsewhere: B. G. Silbernagel and D. C. Johnston, Bull. Am. Phys. Soc. 24, 390 (1979).
[14]D. C. Johnston and H. B. MacKay, Bull. Am. Phys. Soc. 24, 390 (1979); and (unpublished).
[15]L. D. Woolf, D. C. Johnston, H. B. MacKay, R. W. McCallum, and M. B. Maple, J. Low Temp. Phys. 35, 651 (1979).
[16]T. Jarlborg, A. J. Freeman, and T. J. Watson-Yang, Phys. Rev. Lett. 39, 1032 (1977).
[17]A. J. Freeman, T. Jarlborg, and T. J. Watson-Yang, J. Magn. Magn. Mater. 7, 296 (1978).
[18]A. J. Freeman and T. Jarlborg, J. Appl. Phys. 50, 1876 (1979).
[19]G. C. Carter, L. H. Bennett, and D. J. Kahan, *Metallic Shifts in NMR* (Pergamon, New York, 1977), Vol. II, p. 719ff.
[20]A. H. Thompson and B. G. Silbernagel, J. Appl. Phys. 49, 1477 (1978).
[21]V. Jaccarino, B. T. Matthias, M. Peter, H. Suhl, and J. H. Wernick, Phys. Rev. Lett. 5, 251 (1960).
[22]D. C. Johnston, Solid State Commun. 24, 699 (1977).
[23]A. Abragam, *Principles of Nuclear Magnetism* (Oxford University, New York, 1961), pp. 128-131.
[24]J. H. Van Vleck, Phys. Rev. 74, 1168 (1948).
[25]A. Abragam, Ref. 23, pp. 437-442.
[26]P. W. Anderson and P. R. Weiss, Rev. Mod. Phys. 25, 269 (1953).
[27]C. Kittel, *Introduction to Solid State Physics*, 4th ed. (Wiley, New York, 1971), p. 532.
[28]C. Kittel, Ref. 27, p. 452.
[29]P. W. Selwood, *Magnetochemistry*, 2nd ed. (Interscience, New York, 1956), p. 78.
[30]G. C. Carter, L. H. Bennett, and D. J. Kahan, Ref. 19, Vol. I, p. 9.
[31]M. A. Ruderman and C. Kittel, Phys. Rev. 96, 99 (1954); T. Kasuya, Prog. Theor. Phys. 16, 45 and 58 (1956); K. Yosida, Phys. Rev. 106, 893 (1957).
[32]D. C. Johnston and R. N. Shelton, J. Low Temp. Phys. 26, 561 (1977), and references therein.
[33]D. Davidov, A. Chelkowski, C. Rettori, R. Orbach, and M. B. Maple, Phys. Rev. B 7, 1029 (1973).